
Two-Dimensional SSD on OMEGA

The ultimate goal of the LLE uniformity program is to reduce the rms laser-irradiation nonuniformity to the 1%–2% level, which is required for cryogenic implosion experiments on OMEGA. The combination of distributed phase plates (DPP's), two-dimensional (2-D) smoothing by spectral dispersion (SSD), polarization wedges, and beam overlap should be sufficient to reach this goal. We present here a discussion of the mathematical formalism of 2-D SSD with numerical calculations illustrating the levels of uniformity that can be achieved on OMEGA. The initial implementation of 2-D SSD is described, and the initial experimental results for uniformity are compared with theory.

2-D SSD Concept

The level of uniformity that can be achieved with SSD is determined by two factors: bandwidth and spectral dispersion. The amount of bandwidth determines the rate of smoothing, and the amount of spectral dispersion determines the maximum reduction in nonuniformity that can be achieved (as well as the longest spatial wavelength of nonuniformity that can be smoothed). Frequency-tripled glass lasers place constraints on both bandwidth and spectral dispersion. Current techniques for

the high-efficiency frequency tripling of laser light limit the (full-width) bandwidth to 3 Å to 4 Å in the IR for OMEGA. Spatial-filter pinholes in the laser chain limit the spectral spread of the beam to five to ten times the beam's IR diffraction limit. With these constraints, the levels of uniformity required for OMEGA experiments can be achieved using SSD.

The starting point for a description of the uniformity that can be achieved by 2-D SSD is the speckle pattern produced by a phase plate. An example is shown in Fig. 69.1(a). It is characterized by a smooth, well-defined intensity envelope on target. However, superposed on the envelope is highly modulated intensity structure (known as speckle), which is produced by interference between light that has passed through different portions of the phase plate. SSD smoothes this speckle structure in time by progressing through a sequence of many copies of this speckle pattern, each shifted in space, so that peaks of some fill in the valleys of others at different times. When averaged in time, this effect is qualitatively similar to whole-beam deflection: 1-D SSD has the effect of sweeping the beam in only one direction, and 2-D SSD is similar to sweeping the beam in two dimensions.

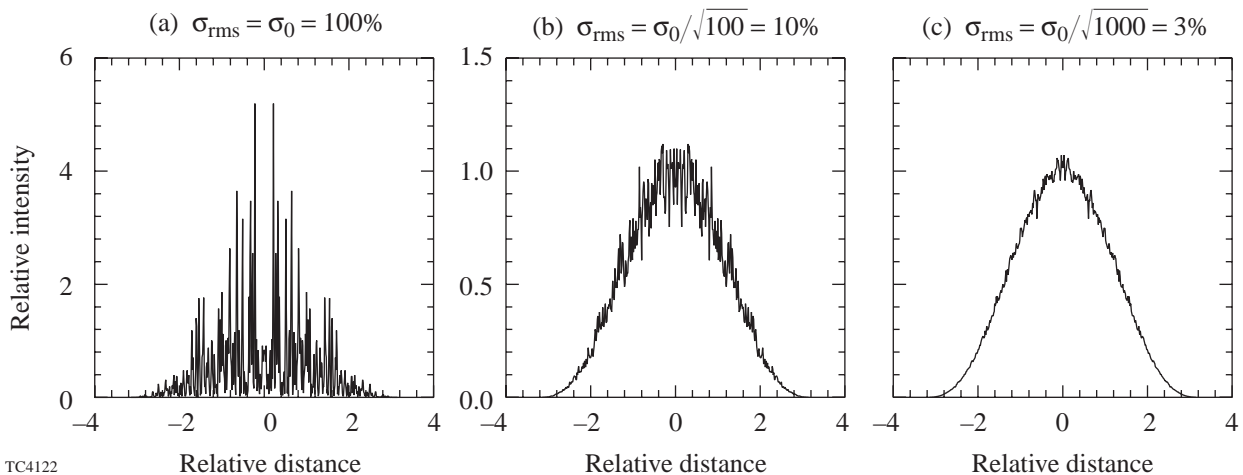


Figure 69.1

The effect of overlapping a large number of statistically different speckle patterns. For a single pattern the rms nonuniformity $\sigma_{\text{rms}} = 100\%$. For N patterns, the rms nonuniformity is reduced by $1/\sqrt{N}$.

The reduction in rms nonuniformity is statistical in nature. Patterns shifted by more than about 1/2 of a speckle width act as entirely different random speckle patterns. The overlap of N random speckle patterns reduces the rms nonuniformity σ_{rms} by $1/\sqrt{N}$. Examples in Figs. 69.1(b) and 69.1(c) show how 100 and 1,000 overlapping speckle patterns reduce the phase plate σ_{rms} of 100% to values of 10% and 3%, respectively. OMEGA will require 2000 to 10,000 of such overlapping patterns, produced as follows: 2-D SSD will provide ~500 of the speckle patterns (for a 1-ns smoothing time); the polarization shifter will provide an additional factor of 2; and multiple-beam overlap will provide another factor of ~4, for a resulting nonuniformity of 1%–2%.

SSD generates these shifted speckle patterns in a two-step process.¹ The beam is passed through an electro-optic modulator, which imposes a small spread of frequencies (bandwidth) upon the laser light. The bandwidth is then spectrally dispersed by means of diffraction gratings. For 1-D SSD, one modulator is used. For 2-D SSD, two modulators (of different frequencies) are used, with diffraction gratings oriented such that each bandwidth is dispersed in a perpendicular direction. Because of the dispersion, each spectral component focuses onto the target in a slightly different position, producing the required shifted speckle patterns (Fig. 69.2).

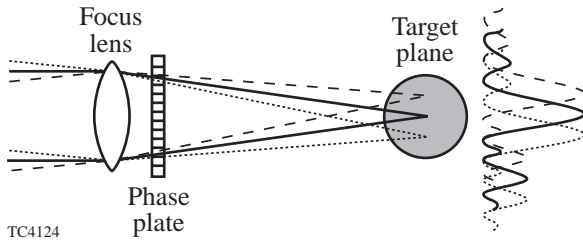


Figure 69.2
Schematic illustrating the use of spectral dispersion to generate overlapping speckle patterns. The different spectral modes are spatially shifted in the target plane. Speckle patterns that are shifted by more than 1/2 of a speckle size are statistically independent.

The spectral dispersion does not reduce the speckle fluctuations instantaneously. It creates an entirely different speckle pattern, but one that changes in time. Interference between the electric fields from different sections of the beam will fluctuate in time because of their different frequencies, and the time-averaged interference approaches zero at a rate inversely proportional to the difference in frequency. As the contributions from interference become small, the time-averaged

uniformity “smoothes” to the result expected from superposing shifted intensity profiles, each corresponding to a different frequency.

The time-averaged uniformity approaches an asymptotic level that is determined by the number of statistically independent speckle patterns (which is generally smaller than the number of spectral components with different frequencies). This depends on the ratio between the maximum spatial shift (S_{max}) that can be produced by the laser and the smallest shift (S_{min}) that will produce statistical smoothing. The maximum spatial shift S_{max} is defined as the full-width distance in the target plane that rays in the laser beam are deflected by SSD dispersion. The smallest shift S_{min} is 1/2 of a speckle size and is given by

$$S_{\text{min}} = F\lambda/D, \quad (1)$$

where F is the focal length, λ is the UV wavelength, and D is the diameter of the focus lens. The maximum shift S_{max} is determined by the maximum angular spread of the light that can propagate through the spatial-filter pinholes of the laser (Fig. 69.3). This can be conveniently expressed as a multiple s of the whole beam diffraction limit (pinhole sizes are often expressed in terms of this parameter). Thus,

$$S_{\text{max}} = s \cdot (2.4 F\lambda/D). \quad (2)$$

Currently, OMEGA pinholes can accommodate $s = 15$, while $s = 30$ is planned for the future. (Note: In this article s is quoted in terms of UV wavelength; if expressed in terms of the IR wavelength, s should be decreased by a factor of 3.) In terms of these parameters, the number of statistically independent speckle patterns (N_{stat}) is

$$N_{\text{stat}} = (S_{\text{max}}/S_{\text{min}})^2 = (2.4 s)^2, \quad (3)$$

where the ratio is squared because 2-D SSD allows spectral shifting in two directions. (This estimate for N_{stat} is somewhat simplified because it assumes that all 2-D SSD modes have different frequencies and are therefore independent; more accurate calculations are given in the next section.) The current and future values of N_{stat} are 1300 and 5000 for OMEGA, which, by itself, should reduce the rms speckle fluctuation to 3% and 1.5%, respectively, in the asymptotic limit. For 1-D SSD, $N_{\text{stat}} = 2.4 s$, with the asymptotic nonuniformity about a factor of 5 larger.

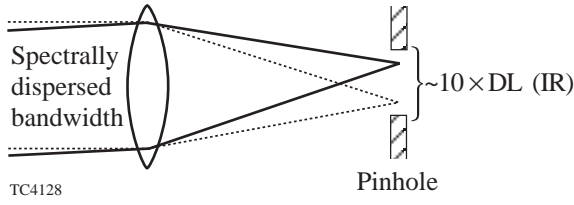


Figure 69.3

Schematic illustrating the limitation imposed by the spatial-filter pinholes on the amount of spectral dispersion that can propagate through the laser chain. Since the minimum separation between modes in the target plane is 1/2 the speckle size, the pinholes provide an upper limit on the number of modes available for smoothing.

For the current OMEGA pinhole size ($s = 15$), $S_{\max} = 76 \mu\text{m}$; thus, the bandwidth and grating dispersion are chosen such that rays from each phase-plate element are deflected $\pm 38 \mu\text{m}$ during an SSD modulation cycle. This is small in comparison with a typical target diameter ($\sim 1 \text{ mm}$); the performance of SSD is thus limited not by the finite target size but by the selection of pinholes in the laser system.

In addition to the asymptotic level of uniformity, the rate of smoothing is of crucial importance. Smoothing must occur before the target can significantly respond to the laser nonuniformity. A rough estimate for the rate of smoothing provided by SSD can be obtained from the following argument. The rms nonuniformity, averaged over time T , will decrease with the number of noninterfering spectral components N_T as $1/\sqrt{N_T}$. (The time-averaged nonuniformity will continue to decrease until $N_T = N_{\text{stat}}$, and then it will asymptote.) The smallest frequency difference $\delta\nu$ for which interference is negligible is roughly $\delta\nu = 1/T$. For a bandwidth $\Delta\nu$, one has $N_T = \Delta\nu/\delta\nu = \Delta\nu T$. Thus, the rms nonuniformity decreases as $1/\sqrt{\Delta\nu T}$. As an example, with $\Delta\nu = 300 \text{ GHz}$ (equivalent to an IR bandwidth of 3 \AA) and $T = 1 \text{ ns}$, one finds $N_T \approx 300$. This value of N_T is less than N_{stat} for a spectral separation of 15 times diffraction limit, so that smoothing will continue beyond 1 ns (but such large smoothing times might be too long to affect target performance).

This rate of smoothing is expected to be fast enough to perform the high-compression experiments planned for OMEGA. When combined with polarization shifters and beam overlap, the resulting nonuniformity will be in the range of 1% to 2% with a smoothing time of $\sim 500 \text{ ps}$. Higher levels of uniformity could be achieved with the development of new technologies for tripling larger bandwidths. New tripling crystals with a larger bandwidth acceptance are under investigation,

as are improved tripling configurations using existing materials. One option under consideration is to vary the bandwidth in time. At early times, when the intensity is low and high irradiation uniformity is critical, the bandwidth would be large. At these intensities the bandwidth acceptance of the tripling crystals is larger, thus maintaining efficiency. Near the peak of the pulse where high tripling efficiency is crucial, but where laser uniformity can be relaxed because of the smoothing characteristics of the plasma atmosphere that has formed around the target, the bandwidth can be reduced.

2-D SSD Formalism and Results

The principal components of 2-D SSD are shown schematically in Fig. 69.4. With this configuration the bandwidth imposed by the two modulators will be dispersed in two perpendicular directions.

The effect of this configuration on the laser's electric field can be determined approximately from the following treatment. The electric field of the laser entering the first diffraction grating can be written as

$$E(t) = E_0(t)e^{i\omega t}, \quad (4)$$

where the spatial dependence has been suppressed, and the pulse-shape dependence is contained in $E_0(t)$. The first grating in Fig. 69.4 will introduce a time shear across the beam in the x direction, which is equivalent to spectral dispersion. (The directions of dispersion will be referred to as x or y and are perpendicular to the direction of propagation. The change in propagation direction produced by each grating is not shown in Fig. 69.4 and is not relevant to the present discussion.) With the time shear, the electric field becomes

$$E_1(t, x) = E_0(t - \beta x)e^{i\omega(t - \beta x)}, \quad (5)$$

where β is related to the grating dispersion ($\Delta\theta/\Delta\lambda$) by

$$\beta = \frac{2\pi}{\omega} \left(\frac{\Delta\theta}{\Delta\lambda} \right). \quad (6)$$

The quantity $D\beta$ (where D is the beam diameter) remains invariant throughout the laser chain as the beam diameter changes size; its value is the time delay across the beam. For parameters at the end of the IR portion of the laser ($\Delta\theta/\Delta\lambda = 31 \mu\text{rad}/\text{\AA}$, $D \approx 30 \text{ cm}$, $\omega \approx 1.8 \times 10^{15} \text{ s}^{-1}$), the time delay $D\beta$ is about 300 ps.

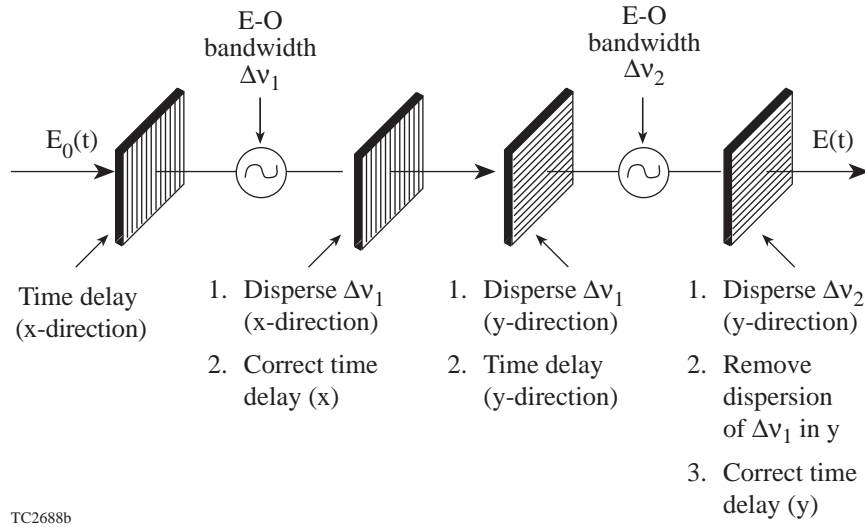


Figure 69.4
Schematic of 2-D SSD, illustrating how the bandwidths from the two modulators are dispersed in perpendicular directions.

The first electro-optic modulator introduces sinusoidal phase-modulated bandwidth to E_1 , with amplitude δ_1 and angular frequency ω_1 . The resulting electric field is

$$E_2(t, x) = E_0(t - \beta x) e^{i[\omega(t - \beta x) + \delta_1 \sin(\omega_1 t)]}. \quad (7)$$

The second grating reverses the time shear of the first and disperses the bandwidth in the x direction:

$$E_3(t, x) = E_2(t + \beta x, x). \quad (8)$$

The third grating introduces a time shear in the y direction, which adds spectral dispersion in that direction. The same time shear, given by β , is used in both x and y directions, although this is not a requirement:

$$E_4(t, x, y) = E_3(t - \beta y, x). \quad (9)$$

Gratings 2 and 3 can be replaced by a single grating oriented at 45° to the gratings shown. The second electro-optic modulator introduces additional bandwidth with parameters δ_2 and ω_2 . At this point the electric field is

$$E_5(t, x, y) = E_0(t - \beta y) \cdot \exp i[\omega(t - \beta y) + \delta_1 \sin \omega_1(t + \beta x - \beta y) + \delta_2 \sin(\omega_2 t)]. \quad (10)$$

(There can be an arbitrary phase difference between the two modulators, but this does not affect uniformity on target and has not been included here.) Finally, the fourth grating reverses the effect that the third grating had on the beam due to the bandwidth imposed by the first modulator, and introduces y dispersion (and a time shear) to the bandwidth from the second modulator. The resulting electric field from this configuration has the bandwidth from the first modulator dispersed only in the x direction, the bandwidth from the second modulator dispersed only in the y direction, and no time shear across the beam:

$$E = E_0(t) \cdot \exp i[\omega t + \delta_1 \sin \omega_1(t + \beta x) + \delta_2 \sin \omega_2(t + \beta y)]. \quad (11)$$

This spectrally dispersed light propagates through the laser chain, through the frequency-tripling crystals and phase plates, and through the focus lenses onto the target. For the bandwidths considered here, the main effect of frequency tripling is that the modulation amplitudes δ_1 and δ_2 are each tripled, as is the laser angular frequency ω . Frequencies at the extremes of the bandwidth will triple less efficiently than those near the center. For current frequency-tripling crystals, the difference in efficiency for bandwidths below $\sim 4 \text{ \AA}$ does not significantly effect the uniformity.

The electric field on target (in the focal plane) is

$$E_F = E_0(t)e^{i3\omega t} \sum_{mn} J_m(3\delta_1)J_n(3\delta_2) \times \text{sinc}(m\gamma_1 + q) \cdot \text{sinc}(n\gamma_2 + p) \times e^{i(m\omega_1 + n\omega_2)t} \times \sum_{KL} e^{-i[2(m\gamma_1 + q)L + 2(n\gamma_2 + p)K + \phi_{KL}]}. \quad (12)$$

This expression includes the effect of the DPP, frequency tripling, and spectral dispersion. Here the notation of Ref. 1 has been used with a generalization to two-dimensional dispersion. For simplicity, the results are written in terms of a two-level phase plate rather than the more general DPP,² which is actually used on OMEGA. The main effect of the more general phase plate is to replace the ‘‘sinc’’ envelope shape by a more general function, but the speckle statistics are very similar. The variables are defined as follows: p and q are dimensionless variables related to y and x by the factor $k_3\Delta/2F$, where k_3 is the wave number of the frequency-tripled fundamental, Δ is the distance between phase-plate elements, F is the focal length, and $\gamma_{1,2} = \omega_{1,2}\beta\Delta/2$. The Bessel functions J_m and J_n are the amplitudes from a Fourier decomposition of the sinusoidal phase modulation. Formally the m - n sum extends to $\pm\infty$, but the contributions from $|m| > 3\delta_1$ and $|n| > 3\delta_2$ are very small. Thus, to a good approximation, the largest spectral modes of interest are given by $m = M \equiv 3\delta_1$ and $n = N \equiv 3\delta_2$. The K - L sum is the factor that describes the phase-plate speckle. The sum is over all phase-plate elements, each having a phase ϕ_{KL} , which is either 0 or π . Note that each spectral component (m, n) has exactly the same speckle structure but is shifted by $m\gamma_1$ in q and by $n\gamma_2$ in p .

These variables have the following physical significance. The phase-plate element size Δ is generally chosen so that the distance between the zeros of the sinc function is slightly larger than the largest target that will be irradiated (to assure good uniformity). Thus, $p, q = \pi$ is characteristic of the target radius. The total spectrally induced spreads in the two directions, as fractions of the target diameter, are approximately $M\gamma_1/\pi$ and $N\gamma_2/\pi$. The total bandwidths in the two directions are $\Delta\nu_1 = M\omega_1/\pi$ and $\Delta\nu_2 = N\omega_2/\pi$. The number of times that the phase modulation repeats across the beam is $\gamma_{1,2}K_{\max}/\pi$, where K_{\max} is the number of phase-plate elements in one direction.

The laser intensity I in the focal plane is given by the square of $|E_F|$:

$$I = I_0(t) \sum_{\substack{mm' \\ nn'}} J_m(3\delta_1)J_{m'}(3\delta_1)J_n(3\delta_2)J_{n'}(3\delta_2) \cdot e^{i(m\omega_1 + n\omega_2 - m'\omega_1 - n'\omega_2)t} \times \text{sinc}(m\gamma + q) \text{sinc}(m'\gamma + q) \times \text{sinc}(n\gamma + p) \text{sinc}(n'\gamma + p) \times \sum_{\substack{KK' \\ LL'}} e^{i2(L'-L)q + i2(K'-K)p} \times \left\{ e^{i2\gamma(m'L' - mL + n'K' - nK) + i(\phi_{K'L'} - \phi_{KL})} \right\}. \quad (13)$$

The final summation has been written in the form of a Fourier decomposition of the speckle nonuniformity with the term in brackets being the Fourier coefficients.

The time-averaged uniformity at time t in the focal plane is

$$\langle I(t) \rangle_T = \frac{1}{T} \int_{t-T/2}^{t+T/2} I(t') dt' \quad (14)$$

for an averaging time T . To examine the smoothing effect of 2-D SSD, it is instructive to evaluate the asymptotic limit of $\langle I \rangle_T$ as $T \rightarrow \infty$. To simplify the result, consider the special case for which (1) $I_0(t)$ is constant; (2) the spectral shifts are sufficiently small that the sinc envelope is not modified; and (3) the modulation frequencies are incommensurate, i.e., $m\omega_1 \neq n\omega_2$ for all integers m and n . The resulting asymptotic uniformity can be written in the following form:

$$\langle I \rangle_\infty = I_{\text{env}}(p, q) \cdot \left[1 + \sum_{k\ell \neq 0} e^{i(2kp + 2\ell q)} C_{k\ell} \cdot R_{k\ell} \right], \quad (15)$$

where I_{env} is the diffraction-limited phase-plate envelope, C is the spatial autocorrelation function for the phase plate, R is the reduction in nonuniformity produced by SSD, and the summation is over the distance between phase-plate elements (i.e., $k = K' - K$ and $\ell = L' - L$). These terms are defined as follows:

$$I_{\text{env}} = I_0 \text{sinc}^2(p) \text{sinc}^2(q) N^2, \quad (16)$$

where N^2 is the number of phase-plate elements,

$$C_{k\ell} = \sum_{KL} e^{i(\phi_{K+k, L+\ell} - \phi_{KL})}, \quad (17)$$

and

$$R_{k\ell} = \sum_{mn} J_m^2(3\delta_1) J_n^2(3\delta_2) e^{i(2\gamma_1 m \ell + 2\gamma_2 n k)}. \quad (18)$$

Using the Bessel function identity

$$\sum_n J_n(3\delta) J_{n+\nu}(3\delta) e^{in\gamma\ell^2} = J_\nu(w) e^{i\nu\theta}, \quad (19)$$

where $w = 6\delta|\sin\gamma\ell|$ and $\sin\theta = (3\delta\sin\gamma\ell)/w$, the SSD reduction factor becomes

$$R_{k\ell} = J_0(6\delta_1 \sin\gamma_1 \ell) \cdot J_0(6\delta_2 \sin\gamma_2 k). \quad (20)$$

In the form of Eq. (15), the nonuniformity structure has been Fourier decomposed in terms of the variables p and q , with the difference between phase-plate elements k and ℓ acting as dimensionless wave numbers. The rms fluctuation is determined by the square of the Fourier coefficients:

$$\sigma_{rms} = \left[\sum_{k\ell} |C_{k\ell} \cdot R_{k\ell}|^2 \right]^{1/2}. \quad (21)$$

The phase-plate result (without SSD) is recovered for $R_{k\ell} = 1$ (for all k and ℓ), in which case the rms nonuniformity is 100%.

The SSD reduction factor depends on the spatial wavelength of the nonuniformity through k and ℓ : For $\gamma_1 \ell < (6\delta_1)^{-1}$ and $\gamma_2 k < (6\delta_2)^{-1}$ the factor $R_{k\ell}$ is approximately 1. When either k or ℓ is small, the factor reduces to the 1-D SSD result. This occurs when the wave vector for the nonuniformity points toward one of the directions of dispersion. Maximum smoothing from 2-D SSD occurs when both k and ℓ are large. Fig-

ure 69.5 shows the reduction factor $|R_{k\ell}|$ using the current OMEGA values ($\delta_1 = 5.1$, $\delta_2 = 4.6$) for the cases when one wave number is kept small ($\ell = 0$) and for the case when the wave vector is at 45° to the direction of dispersion ($\ell = k$). The improved smoothing in the second case, corresponding to two-dimensional smoothing of the nonuniformity in both directions, is apparent.

The condition that there is no significant smoothing for $6\delta_1 \gamma_1 \ell < 1$ has a simple physical interpretation. The factor $6\delta_1 \gamma_1$ is the total spectrally induced shift S_{\max} in the target plane in units of q . The parameter ℓ is related to the wavelength of nonuniformity $\Delta\lambda$ by $\Delta\lambda = \pi/\ell$ (again in units of q). Thus, the largest wavelength of nonuniformity that will be smoothed by SSD is approximately πS_{\max} . In other words, the spectral shift must be a significant portion of the nonuniformity wavelength for smoothing to occur.

The amount that the speckle pattern is shifted can be doubled (in one direction) by means of a polarization shifter.^{3,4} This is illustrated in Fig. 69.6 for the shifter currently under investigation at LLE, a birefringent wedge of KDP placed after the frequency-tripling crystals. The birefringence of KDP separates the laser beam into two orthogonal polarizations, which are deflected by the wedge through slightly different angles. (Alternatively, a liquid-crystal wedge could be used. Depending on the type of liquid crystal, the orthogonal polarizations could be linear or circular.) The two speckle patterns produced on target are spatially displaced, thus doubling the number of independent speckle patterns. The most effective way to use this technique is to disperse the polarization over a distance larger than the spectral dispersion produced by SSD. In this way, the polarization shift smoothes out modes of nonuniformity that are not smoothed by SSD, and overlap between the two techniques is avoided.⁵ The reduction

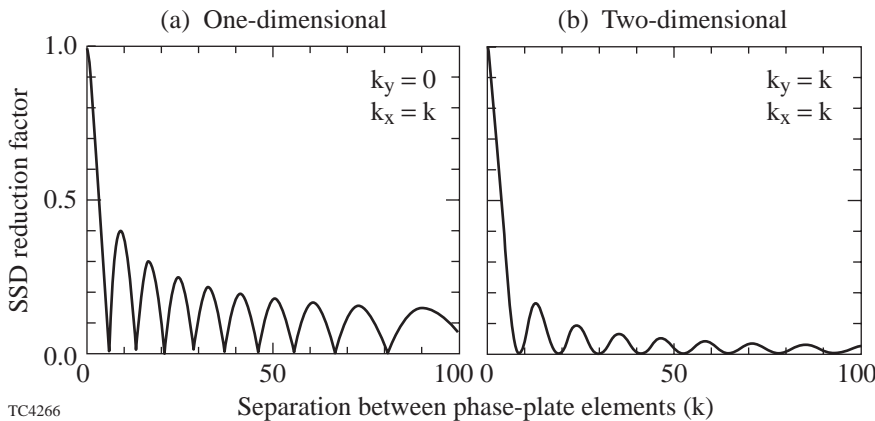


Figure 69.5

The absolute value of the 2-D SSD reduction factor as a function of nonuniformity wave vector (or equivalently the separation k between phase-plate elements). (a) The wave vector is along one of the dispersion directions. The reduction is the same as for 1-D SSD. (b) The wave vector is at 45° , resulting in the maximum 2-D reduction.

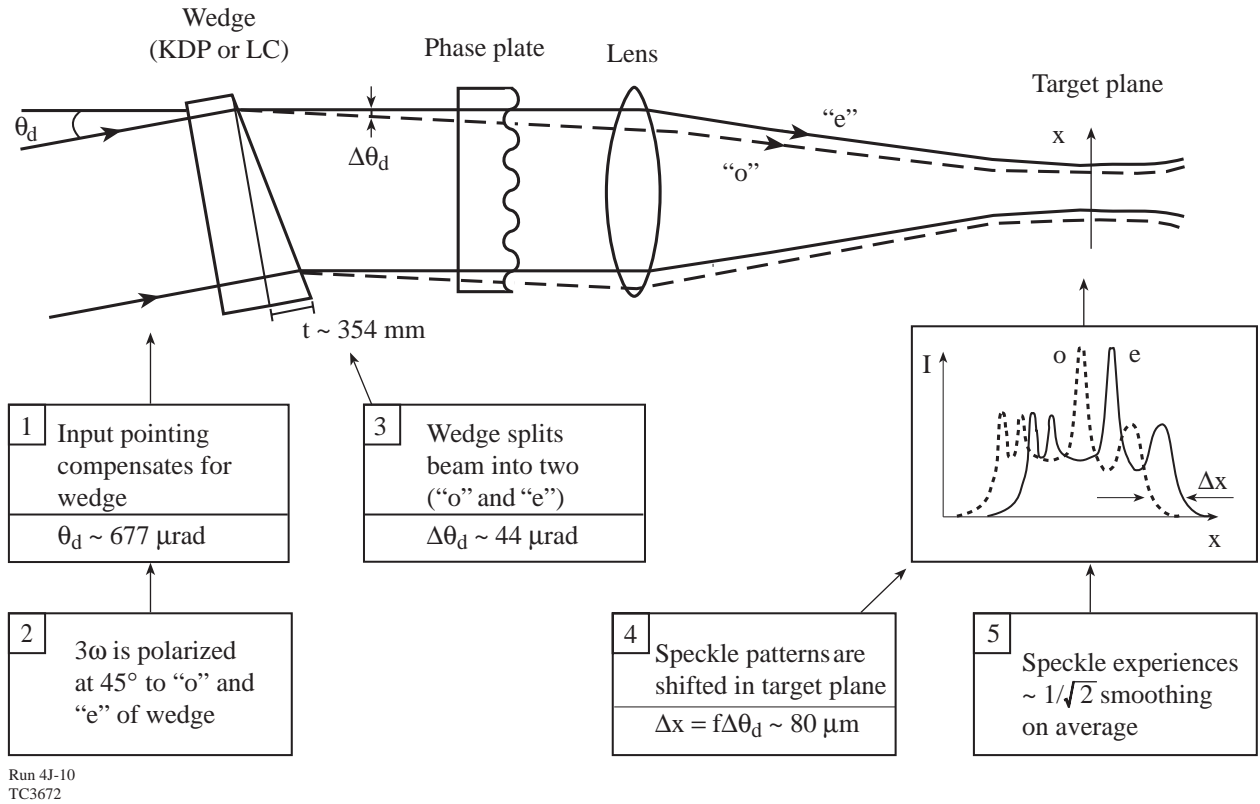


Figure 69.6 Principle of the (birefringent) polarization wedge. The laser beam is split equally into two orthogonal polarizations (“o” and “e”), which are deflected by the wedge through slightly different angles. This results in two spatially displaced speckle patterns in the target plane with orthogonal polarizations, which add in intensity rather than electric field, providing an instantaneous reduction of $1/\sqrt{2}$ in the rms nonuniformity.

in nonuniformity resulting from the polarization shifter is instantaneous because there is no interference between the two polarizations.

The predicted improvement in uniformity produced by 2-D SSD on OMEGA is shown in Fig. 69.7 as a function of the smoothing time. The results are for multiple overlapping beams on a spherical target and thus include the smoothing effect of overlapping beams. Two cases are presented. One shows the results for the current implementation of 2-D SSD in which 1.5 Å of bandwidth is dispersed in each direction. The second case shows the result of doubling the bandwidth in one direction and adding polarization dispersion in the second. This case achieves the uniformity goal of OMEGA, namely reaching the 1%–2% rms level within a smoothing time of less than 500 ps.

Implementation of 2-D SSD

2-D SSD was implemented on OMEGA in January 1996. An aggressive optical design program showed that 2-D SSD

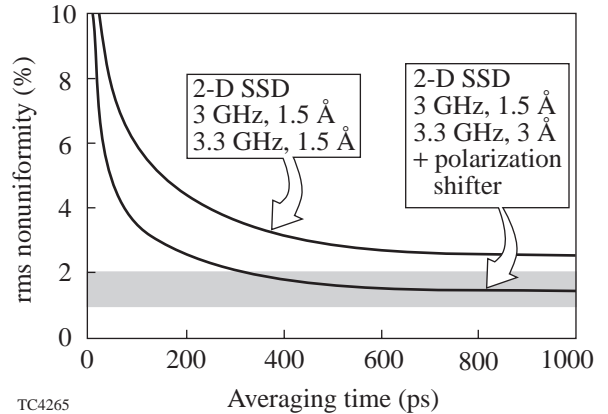


Figure 69.7 Reduction in rms nonuniformity as a function of smoothing time for multiple beam overlap on a spherical target, using the 60-beam OMEGA geometry. Spherical harmonic modes up to $\ell = 500$ have been considered with no additional smoothing assumed in the plasma atmosphere around the target. The lower curve corresponds to a higher bandwidth in one direction and the inclusion of polarization shifters.

could be implemented over roughly the same time interval that was originally planned for 1-D SSD. However, it was important to adopt a conservative strategy with regard to bandwidth during the time that the operating characteristics of the new laser and SSD were being studied, because spectrally dispersed bandwidth can introduce intensity fluctuations that can damage laser optical components. As such, the initial implementation of 2-D SSD used bandwidths of only 1.5 \AA and 0.75 \AA . The initial results presented in this section were generated with these bandwidths. The bandwidth has recently been increased to 1.5 \AA in each direction. To accommodate the increased dispersion of the beam, it has been necessary to enlarge one spatial-filter pinhole in the driver and to enlarge the second SSD modulator crystal. Future plans call for an increase in pinhole diameters later in the laser chain to allow the propagation of up to 3 \AA of bandwidth.

A far-field image of the beam, after the final set of gratings, is shown in Fig. 69.8. Although the individual spectral components can not be seen in this figure, the two-dimensional dispersion is clearly evident. The extremes of the spectrum are the most intense portions for sinusoidal phase modulation. This is seen in the corners of the figure. The two directions of dispersion are not exactly orthogonal due to a 6° misalignment of the periscope that takes the beam out of the pulse generation room (PGR), but this has no effect on the irradiation uniformity on target. The amount of dispersion in each direction is proportional to the bandwidth from each modulator.

Images of the final beam profile,⁶ in an equivalent target plane (ETP), are shown in Fig. 69.9. These images are for a single beam profile and therefore take no account of the additional smoothing achieved by beam overlap. The first

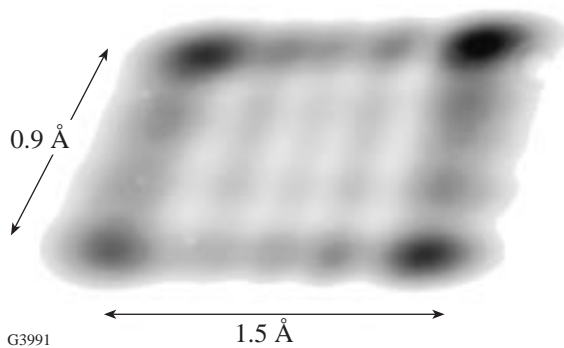


Figure 69.8

A far-field image of the beam (after the final diffraction gratings) showing that the two-dimensional dispersion of the beam is proportional to the bandwidth applied by each modulator.

image [Fig. 69.9(a)] shows the frequency-tripled beam without a phase plate or SSD. The intensity nonuniformity is the result of phase aberrations that have accumulated throughout the laser chain. Figure 69.9(b) shows the improvement produced by a phase plate. A well-defined intensity envelope has been established, but superposed on the envelope is highly modulated speckle. Figure 69.9(c) shows smoothing of the speckle by 1-D SSD, for which the bandwidth is turned on in one modulator and off in the other. Both combinations are shown. The “stripes” in the images show the direction of spectral dispersion. Nonuniformity perpendicular to the dispersion is not smoothed. Finally, the last image [Fig. 69.9(d)] shows the improved smoothing produced by two-dimensional dispersion. Note that the “stripes” have now been eliminated.

These images were time integrated over the laser pulse. The uniformity achieved is characteristic of an SSD smoothing time roughly equal to the pulse width, which was $\sim 1 \text{ ns}$ for this experiment. The rms fluctuations of the intensity around smooth envelopes are listed in Table 69.I, which gives both the measured and theoretically predicted values. A large part of the improved uniformity for 2-D SSD compared with 1-D SSD (a factor of ~ 2) is related to the smoothing duration: 1-D SSD reaches an asymptotic level of uniformity after $\sim 300 \text{ ps}$; 2-D SSD continues to smooth throughout the entire time of the pulse (1 ns). There is an increased bandwidth for 2-D SSD (due to contributions from both modulators), but this has a much smaller effect on the improved uniformity than the increased smoothing duration, for this example.

Very recently a prototype KDP polarization wedge has been tested on OMEGA. One-dimensional lineouts through equivalent-target-plane (ETP) images (Fig. 69.10) show that the predicted $\sqrt{2}$ uniformity improvement is indeed obtained.

Table 69.I: rms nonuniformity for the single-beam images in Fig. 69.9, compared with the theoretically predicted values (when averaged over the 1-ns pulse).

Image	Bandwidth (\AA)	Measured rms	Calculated rms
(b)	0	0.96	0.98
(c)	0.75, 0	0.27	0.28
(c)	0, 1.5	0.24	0.21
(d)	0.75, 1.5	0.12	0.11

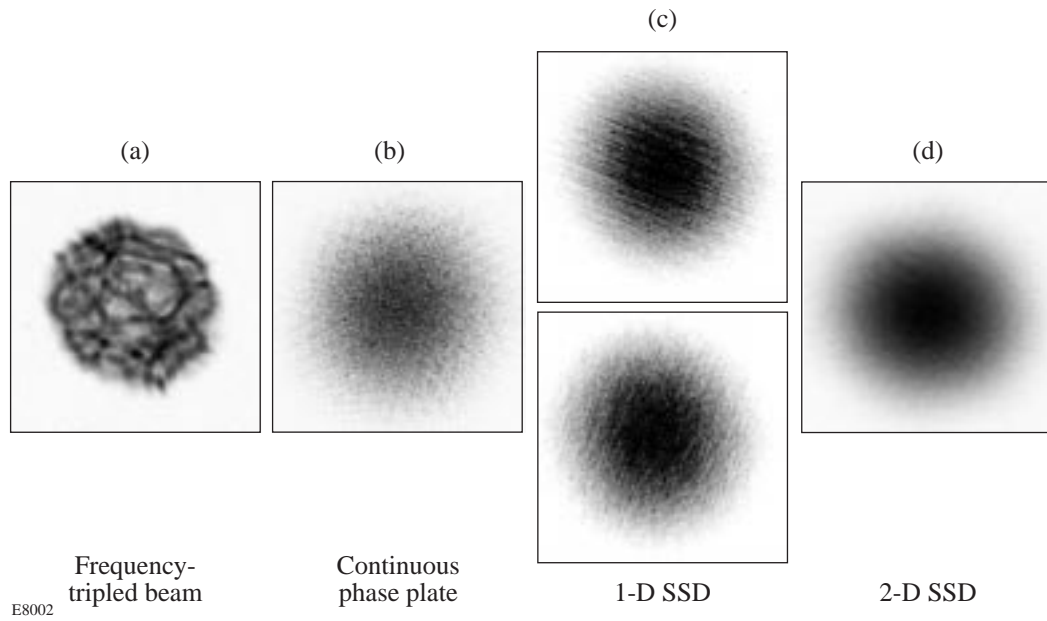


Figure 69.9

Equivalent-target-plane images, integrated over the ~ 1 -ns pulse width, of a single OMEGA beam with four levels of smoothing: (a) unsmoothed, frequency-tripled; (b) phase plate, no bandwidth; (c) bandwidth in only one modulator; (d) bandwidth in both modulators.

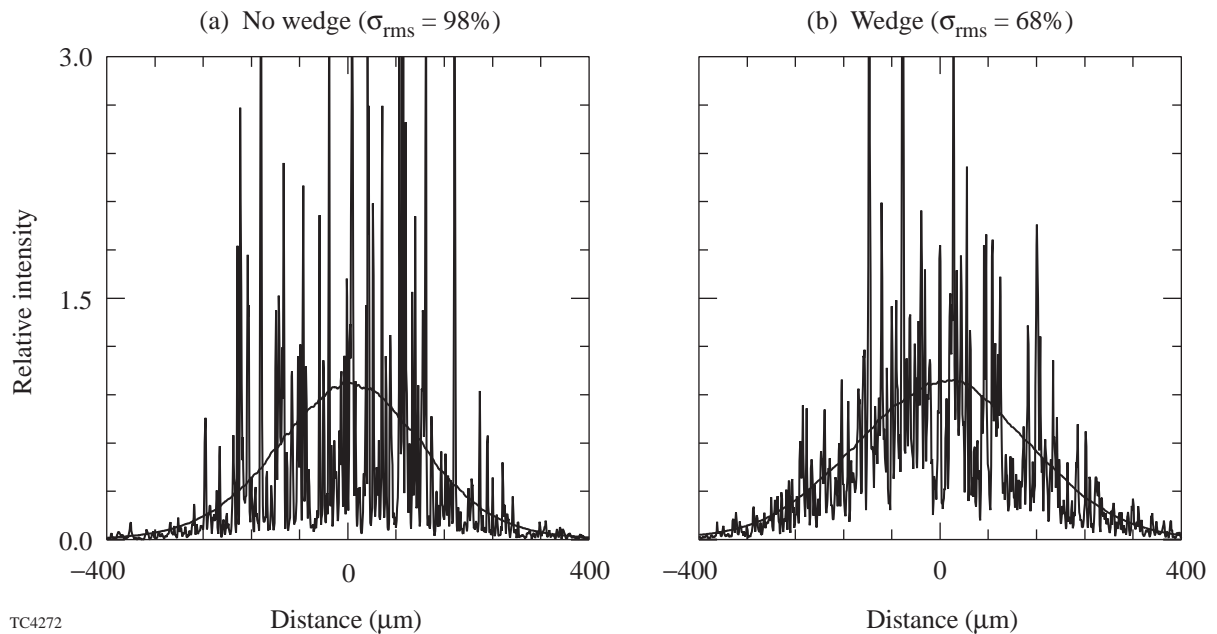


Figure 69.10

One-dimensional lineouts of the ETP images on OMEGA produced (a) without a polarization wedge and (b) with a polarization wedge. The measured rms nonuniformities of $\sigma_{\text{rms}} = 98\%$ and 68% , respectively, demonstrate the predicted $\sqrt{2}$ uniformity improvement made possible by the wedge.

ACKNOWLEDGMENT

This work was supported by the U.S. Department of Energy Office of Inertial Confinement Fusion under Cooperative Agreement No. DE-FC03-92SF19460, the University of Rochester, and the New York State Energy Research and Development Authority. The support of DOE does not constitute an endorsement by DOE of the views expressed in this article.

REFERENCES

1. S. Skupsky, R. W. Short, T. Kessler, R. S. Craxton, S. Letzring, and J. M. Soures, *J. Appl. Phys.* **66**, 3456 (1989).
2. Laboratory for Laser Energetics LLE Review **45**, NTIS document No. DOE/DP40200-149, 1990 (unpublished), p. 1
3. T. J. Kessler, Y. Lin, J. J. Armstrong, and B. Velazquez, in *Laser Coherence Control: Technology and Applications*, edited by H. T. Powell and T. J. Kessler (SPIE, Bellingham, WA, 1993), Vol. 1870, p. 95.
4. Y. Lin, T. J. Kessler, and G. N. Lawrence, *Opt. Lett.* **20**, 864 (1995).
5. R. S. Craxton and S. Skupsky, *Bull. Am. Phys. Soc.* **40**, 1826 (1995).
6. T. R. Boehly, R. L. Keck, C. Kellogg, J. H. Kelly, T. J. Kessler, J. P. Knauer, Y. Lin, D. D. Meyerhofer, W. Seka, S. Skupsky, V. A. Smalyuk, S. F. B. Morse, and J. M. Soures, presented at the *Second Annual International Conference on Solid State Lasers for Application to Inertial Confinement Fusion (ICF)*, Paris, France, 22–25 October 1996.